Dynamic properties of micro-magnetic noise in soft ferromagnetic materials

A. Stupakov[a,*], A. Perevertov[a]

[a]*Institute of Physics of the Czech Academy of Sciences, Na Slovance 2, 18221 Prague, Czechia*

Abstract

Dynamic response of magnetic hysteresis, magnetic Barkhausen noise and magneto-acoustic emission in a soft ribbon and electrical steels was studied comprehensively. The measurements were performed under controllable magnetization conditions: sinusoidal/triangular waveforms of the magnetic induction and a triangular waveform of the magnetic field. Magnetizing frequency was varied in a wide range: $f_{mag} = 0.5 - 500$ and $0.1 - 100$ Hz for the ribbon and the electrical steels, respectively. Magnetization amplitude was fixed on a near-saturation level $H_{max} \simeq 100$ A/m. Barkhausen noise signal was detected by a sample-wrapping/surface-mounted coil and differently filtered. It was found that intensity of the Barkhausen noise rises approximately as a square root function of the magnetizing frequency. Whereas, level of the magneto-acoustic emission follows the hysteresis loss trend with an additional linear term (classical loss component).

Keywords: Magnetization dynamics, Barkhausen noise, Magneto-acoustic emission, Magnetic hysteresis, Electrical steel

*Corresponding author. Tel: +420 26605 2114
E-mail: stupak@fzu.cz, URL: www.fzu.cz/˜stupak

1. Introduction

The classical problem of macroscale magnetization dynamics in conventional ferromagnetic materials has not been fully understood so far. In particular, magnetic hysteresis in soft magnetic materials is commonly discussed in terms of a phenomenological loss-separation model in spite of growing criticism of dubious theory assumptions for a classical loss component and of unclear nature of an excess loss [1, 2]. Promising direction of research that should contribute in elucidation of this classical problem is investigation of the magnetization dynamics on a microscale level by measuring Barkhausen noise (BN) and magneto-acoustic emission (MAE). The BN/MAE signals originate from irreversible motion of the magnetic domain walls (DW) and are detected in the form of magnetic/acoustic impulses. Principal distinction between BN and MAE is that the motion of the 180° DWs should not cause any change of the magneto-elastic energy and therefore should not contribute to MAE [3, 4]. Local jumps of the magnetic DWs between material pinning sites such as grain boundaries, inclusions and defects are damped by microeddy currents, which give a considerable contribution to the hysteresis losses [5]. Thereby, acquiring extensive knowledge about the magnetization process on the microscopic scale builds a necessary base for deeper understanding of the dynamic properties and for better prediction of the magnetic losses in electrical transformers and motors.

Dynamic properties of BN/MAE have been scantily investigated so far. This is especially true for the measurements under controllable magnetization conditions providing physically interpretable results [4, 6]. In this work, we first present the dynamic data for a nanocrystalline soft ribbon with

a specific combination of the magneto-mechanical properties making this investigation especially attractive. The principal issue is that a tiny thickness of the ribbon and its high electrical resistivity suppress eddy currents and ensure the homogeneous BN detection. Moreover, the long ribbon can be homogeneously magnetized in a solenoid up to high magnetizing frequencies; and its magnetic field can be easily controlled using the magnetizing current. To ensure consistency of the data and profound analysis of the magnetization dynamics, the measurements are additionally performed for soft electrical steels in another magnetizing configuration.

2. Experimental

2.1. Ribbon

The measurements were performed for an as-cast nanocrystalline Hitperm ribbon with the following composition: $Fe_{54}Co_{27}Nb_7B_{12}$ [7]. It was chosen because of the similar grain structure as industrial ferromagnetic steels. To receive evidence that the data obtained for this ribbon demonstrate a general trend, other ribbons from the same Hitperm series with different Fe-Co composition and a few industrial samples were additionally tested. The tested ribbon was 1 m long, 7 mm wide and 10 μm thick. It was magnetized inside a 30-cm long solenoid; the magnetic field H was calculated from the current in the solenoid winding. A sample-wrapping coil of 4 cm length and 2700 turns was positioned in the solenoid center to estimate the magnetization and the BN signal. For this measurement configuration, a considerable air induced component $\sim dH/dt$ was digitally compensated to evaluate the magnetic polarization J. The hardware details and the set-up

scheme were described in [7]. The magnetization waveform was controlled by a digital feedback with a combined phase-amplitude adjustment, details can be found in [8]. Magnetization conditions, namely the sinusoidal/triangular waveforms of the magnetic polarization $J(t)$ or the triangular waveform of the magnetic field $H(t)$, were controlled in a wide range of the magnetizing frequency $f_{mag} = 0.5 - 500$ Hz. The measurements without the $J(t)/H(t)$ control, namely at the sinusoidal/triangular waveforms of the magnetizing voltage $V(t)$, were also recorded. Magnetization amplitude was fixed on a near-saturation level of $J_{max} = 0.9$ T or $H_{max} = 100$ A/m.

In addition to the measurement with the sample-wrapping coil, BN was alternatively recorded by a small surface-mounted coil also placed in the central part of the solenoid. It was a bobbin coil of 1 cm diameter with 800 turns and a pen-type core of ferrite. Its resonance frequency was about 60 kHz. The BN signal measured by both coils at different magnetization conditions was filtered within three bandwidths 2–40, 10–40 and 40–80 kHz. MAE was detected by a piezoelectric transducer from Dunegan/Endevco, type S9204, placed again in the solenoid center. The amplified MAE signal was filtered in a 100–300 kHz range; the resonance frequency of the MAE transducer was about 150 kHz [4]. The BN/MAE signals were sampled at a 2 MS/s rate.

2.2. Electrical steels

Industrial electrical steels, two grain-oriented (GO) grades and one non-oriented (NO) steel with distinct magnetic parameters, were chosen for the measurements. Steel strips of the Epstein dimensions $300 \times 30 \times 0.25 - 0.5$ mm were magnetized along the rolling direction by a U-shaped transformer yoke

of the same length and width through a 3 mm air gap; two magnetizing coils were positioned on the yoke poles. The tangential component of the surface magnetic field was measured directly by a Hall sensor at 1.5 mm above the yoke-free sample side. This method of surface field determination ensured a good measurement accuracy for the magnetically open configuration used. By introducing the air gap, a total inductance of the magnetizing circuit decreased, which stabilized the feedback procedure. For this configuration, the air induced component $\sim dH/dt$ was negligible, so the magnetic induction $B = \mu_0 H + J$ was estimated directly by a sample-wrapping coil with 100 turns. Waveform of $B(t)$ was adjusted to the sinusoidal/triangular shapes in a $f_{mag} = 0.5 - 100$ Hz range; additional measurements at the sinusoidal $V(t)$ waveform were conducted. Magnetization amplitudes were $B_{max} =$ 1.5 and 1.2 T for the GO and the NO steels, respectively. Accuracy of the measurement configuration and efficiency of the digital feedback were comprehensively discussed in [8].

BN was detected similarly by the sample-wrapping coil and a bigger surface-mounted coil placed in the central part of the strips. It was a bobbin coil of a 16 mm diameter with 1000 turns of fine copper wire inside a Cu-shielded grounded case. A core with a 4×4 mm cross-section was made from a laminated GO steel and gently pressed by a spring to the strip surfaces. A resonance frequency of this coil with the GO core was about 120 kHz [9]. The BN signal was filtered within three bandwidths 2–70, 20–100 and 70–170 kHz. The MAE signal was detected by the same Dunegan transducer and filtered in a 100–500 kHz range.

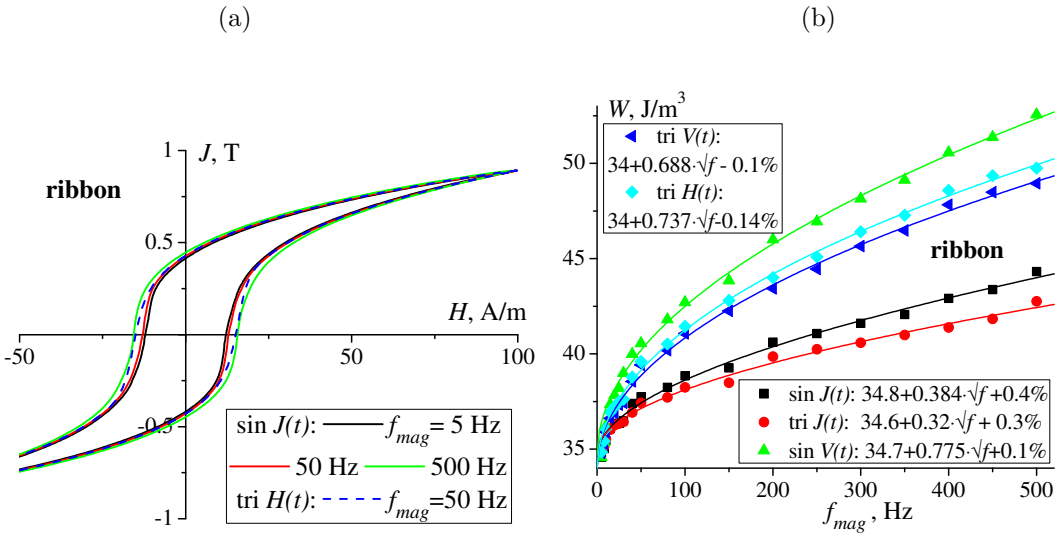

Figure 1: (a) Typical hysteresis loops $J(H)$ obtained for the tested Hitperm ribbon at the different magnetizing waveforms and frequencies. (b) Dependence of the hysteresis loss W on the magnetizing frequency f_{mag} for the same ribbon at the different magnetizing waveforms. Relations are fitted by the loss-separation function with the negligible linear coefficients.

3. Results

3.1. Ribbon

Typical hysteresis loops measured under the sinusoidal waveform of the magnetic polarization $J(t)$ at three magnetizing frequencies $f_{mag} = 5$, 50 and 500 Hz are shown in Fig. 1(a) together with the loop measured at the triangular field $H(t)$ and $f_{mag} = 50$ Hz. The loops become slightly wider with increasing f_{mag}; dc coercive field $H_c \simeq 12$ A/m. Figure 1(b) presents dependence of the hysteresis loss W on the magnetizing frequency for the different magnetizing waveforms. The loss dependence for the triangular voltage $V(t)$ and field $H(t)$ are very close to each other because the field generated inside

the solenoid is nearly proportional to the magnetizing voltage (the circuit resistance prevails over its inductive reactance), i.e. $H(t) \sim I(t) \approx V(t)$. Other relations are quite different, but all of them are fitted well by the loss-separation formula $W = W_{dc} + a \cdot \sqrt{f_{mag}} + b \cdot f_{mag}$, where W_{dc} is an extrapolated static loss at zero f_{mag}. The classical linear term $W_{cl} = b \cdot f_{mag}$ is derived from the Maxwell equations under dubious assumptions that a thin and infinite sheet with constant permeability is magnetized unidirectionally and homogeneously. There is still debate about the origin of the square root term, so-called excess loss $W_{ex} = a \cdot \sqrt{f_{mag}}$, which was added to fit the experimental loss dependence for the electrical steels [1, 2]. The least-square fittings of the experimental loss dependence are shown by the corresponding lines. Graph labels give the fitting formulas with the linear coefficient b presented as a percentage ratio to the square root coefficient b/a; the following linear term f_{mag} is omitted for the sake of simplicity (e.g. a formula $2 + 10 \cdot \sqrt{f} + 1\%$ in the label means the fitting $2 + 10 \cdot \sqrt{f_{mag}} + 0.1 \cdot f_{mag}$). It should be noted that the used coefficient ratio b/a does not agree with a corresponding term ratio $W_{cl}/W_{ex} = (b/a) \cdot \sqrt{f_{mag}}$. Two terms of the loss-separation formula become comparable $W_{cl} = W_{ex}$ at a critical magnetizing frequency $f_{cr} = (a/b)^2$; so the linear term contribution is negligible in the considered f_{mag} range for the ratio b/a varying on a common error level of a few percents (for b/a = 1, 2 and 5 %, f_{cr} = 10, 2.5 and 0.4 kHz, respectively). For the thin ribbons, the classical linear component W_{cl} is known to be negligible [1, 5]. This is also proved by our data: the ratio b/a reaches a maximal value 0.4% for the sinusoidal $J(t)$. Pearson correlation coefficients of the fits equal $R = 0.992$ for the controlled $J(t)$ and $R = 0.997$ for the

(a) (b)

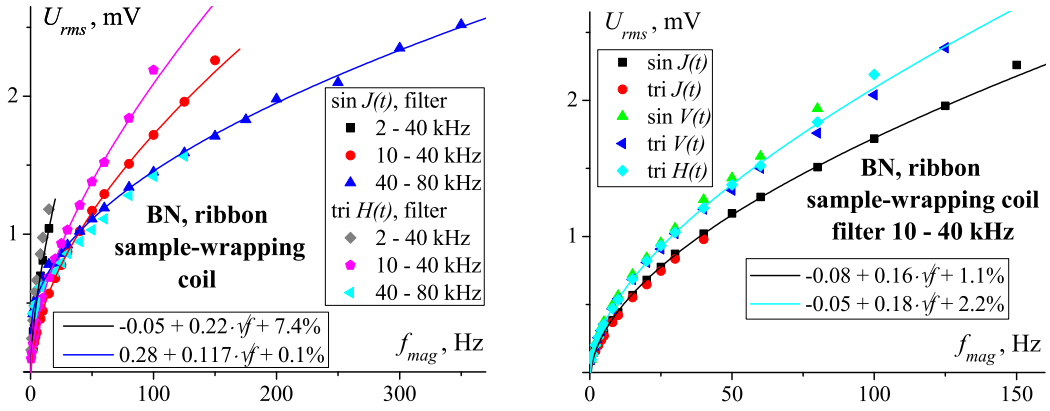

Figure 2: Dependence of the rms value U_{rms} of BN on the magnetizing frequency f_{mag}: (a) for all filtering bandwidths and two magnetizing waveforms, the sinusoidal polarization $J(t)$ and the triangular field $H(t)$; (b) for the medium filtering bandwidth 10–40 kHz and all magnetizing waveforms. The BN signal from the tested Hitperm ribbon is detected by the sample-wrapping coil. Representative relations are fitted by the same loss-separation function with the linear coefficients showed in the labels as the percentage ratio b/a.

other waveforms.

Figure 2 presents similar dynamic dependence of the rms intensity U_{rms} of the one-cycle BN signal detected by the sample-wrapping coil. Low-frequency hysteresis component distinctly distorts the BN output, when f_{mag} value reaches $\sim 1\%$ of a low cutoff frequency of the band-pass filter. Therefore, the measurements at the low filtering bandwidth 2–40 kHz are not representative enough. Constant terms of the loss-separation fits U_{dc} are relatively high: 0.05–0.08 mV for the two lower filtering bandwidths and 0.28 mV for the 40–80 kHz bandwidth. Level of a background noise can be estimated at the saturation regions, where the BN activity is minimal, i.e. as $U_{rms}(H_{max} \simeq$

144 $\pm$100 A/m), or by reading the empty BN response without applying the
145 voltage into the magnetizing coil, i.e. as $U_{rms}(H \equiv 0)$. Thus determined
146 background noise is several times lower than U_{dc} and also dependent on the
147 filtering: for the two lower bandwidths, the background noise level is about
148 0.01 mV; for the 40–80 kHz bandwidth, it is 0.1 mV [6, 10]. Shape of the
149 magnetizing waveform has a qualitatively similar impact on the rms value
150 and the hysteresis loss: the sinusoidal $V(t)$ and the triangular $J(t)$ give the
151 maximal and the minimal values, respectively. However, quantitatively the
152 waveform shape influence is weaker for U_{rms}. For the two lower filtering
153 bandwidths, the U_{rms} relations divide into two groups for the data obtained
154 with and without the $J(t)$ control (see Fig. 2(b)). However, the difference
155 between these two groups vanishes for the higher filtering bandwidth 40–
156 80 kHz (see Fig. 2(a)). The relative linear coefficients of the loss-separation
157 fits are slightly higher than those for the hysteresis loss: $b/a \simeq 1 - 2\%$ for
158 the medium filtering bandwidth 10–40 kHz, which is a still negligible level.
159 For the high filtering bandwidth 40–80 kHz, the linear coefficient is even
160 smaller by an order of magnitude $b/a \simeq 0.1\%$. Correlation coefficients of the
161 fits are $R = 0.9998$ and 0.9989 for the medium and the high bandwidths,
162 respectively.

163 Figure 3 presents similar dependence of the rms value U_{rms} of BN recorded
164 by the surface-mounting coil with the different filtering bandwidths. Interfer-
165 ence of the low-frequency hysteresis contribution is significantly smaller for
166 the detection by the surface coil, so the measurements with the low filtering
167 bandwidth 2–40 kHz can be performed up to $f_{mag} \simeq 50$ Hz (see Fig. 3(a)).
168 The loss-separation fits of these relations with the correlation coefficients

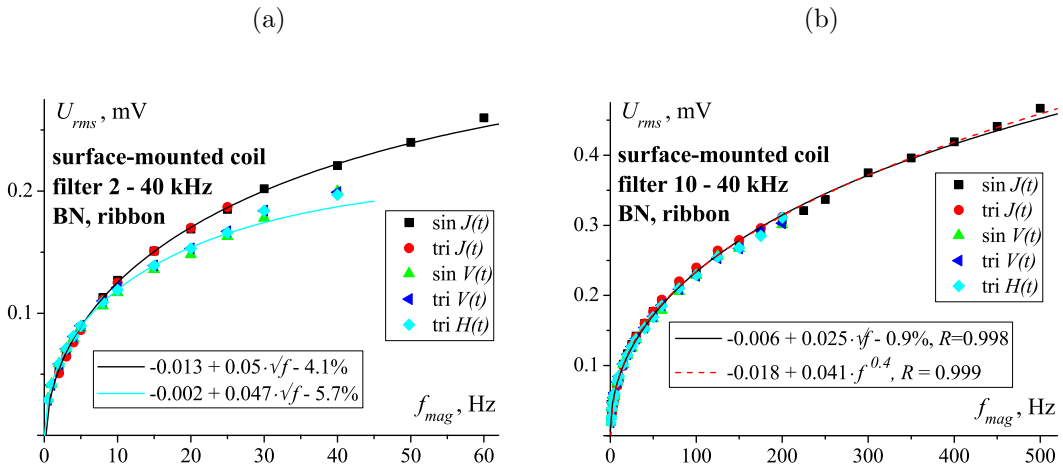

Figure 3: Dependence of the rms value U_{rms} of BN on the magnetizing frequency f_{mag} for all magnetizing waveforms and two filtering bandwidths: (a) 2–40 kHz; (b) 10–40 kHz. The BN signal from the tested Hitperm ribbon is detected by the surface-mounted coil. Representative relations are fitted by the same loss-separation function with the linear coefficients showed in the labels as the percentage ratio b/a. In (b) the relation is additionally fitted by a power function.

$R = 0.9998$ give the negative linear coefficients $b/a \sim -5\%$. The rms relations divide into two similar groups with different dependence on the magnetizing waveform shape. However, the group with the sinusoidal/triangular $J(t)$ demonstrates higher rms values at $f_{mag} > 10$ Hz in contrast to the results obtained with the sample-wrapping coil (compare Figs. 2(b) and 3(a)). This waveform-induced difference between the rms dependence vanishes at the higher cut-off frequency of the filter (see Fig. 3(b)). The loss-separation fitting results in a negative linear coefficient again, but of a smaller negligible level $b/a \sim -1\%$. An alternative power-law fitting gives a similar curve with the similar correlation coefficient $R \simeq 0.999$, but the resulting power term $f_{mag}^{0.4}$ is rather far from the expected $f_{mag}^{0.5}$ [11, 12]. Constant terms of the fits U_{dc} can be again higher than the background noise, whose level is ~ 3 μV for both filtering bandwidths.

Figure 4 presents the discrete Fourier spectra of the BN signals detected by both coils at different magnetizing conditions [9, 13]. For better visualization, the spectra obtained at the higher magnetizing frequencies $f_{mag} = 5 - 50$ Hz in Fig. 4(a) are normalized to a level of the original 2 Hz spectrum on the assumption that the rms magnitude increases according to the square root of the magnetizing frequency, i.e. the spectra are divided by $U_{rms}/\sqrt{f_{mag}/2}$. Such f_{mag}-normalized spectra differ in a low-frequency region up to $f \leq 20$ Hz. This deviation of the spectra from the $U_{rms} \sim \sqrt{f_{mag}}$ behavior at low frequencies results in the negative linear term of the loss-separation fitting in Fig. 3(a). Moreover, only this low-frequency spectral region is sensitive to variations of the magnetizing waveform (see Fig. 4(b)) [6]. The same f_{mag}-normalization of the spectra recorded by the sample-wrapping coil (not

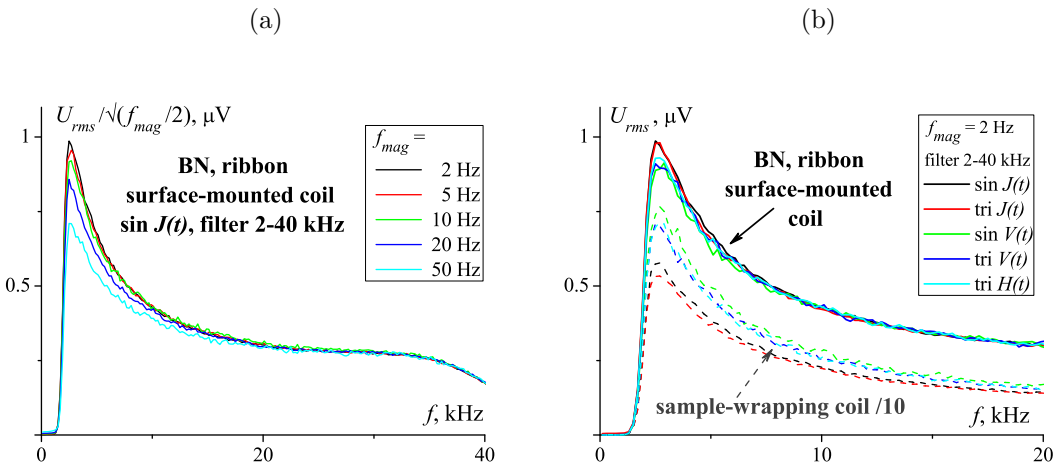

Figure 4: Fourier power spectra of the BN signals from the Hitperm ribbon recorded by the surface-mounted coil at: (a) the sinusoidal polarization $J(t)$ and different magnetizing frequencies $f_{mag} = 2-50$ Hz; (b) different magnetizing waveforms and fixed $f_{mag} = 2$ Hz. The filtering bandwidth is 2–40 kHz. In (a) the spectra for $f_{mag} = 5-50$ Hz are normalized to the 2 Hz spectrum on the assumption of the square root rise with the magnetizing frequency $U_{rms}/\sqrt{f_{mag}/2}$. In (b) the similar spectra recorded by the sample-wrapping coil are shown by the corresponding dashed lines. They are reduced by an order of magnitude to fit the same scale.

shown in the graph) gives similar spectra deviation in the low-frequency region, but of the opposite sign. This logically leads to the positive linear term of the loss-separation fitting in Fig. 2(a). This low-frequency region up to $f \leq 20$ kHz is also sensitive to variations of the magnetizing waveform, however, the spectra obtained with and without the $J(t)$ control are clearly detached for the sample-wrapping data. Next difference between the spectra for both coils is that the spectral magnitudes for the sinusoidal/triangular $J(t)$ are smaller than those obtained without the $J(t)$ control in accordance with the rms dependence in Fig. 2(b).

Figure 5(a) demonstrates a nearly linear correlation between the BN rms values and the hysteresis losses at ac magnetizing frequencies $f_{mag} > 10$ Hz. Number of the individual BN pulses over a magnetization cycle hyperbolically drops with magnetizing frequency (see Fig. 5(b)) [4, 10]. Qualitatively same results are obtained for other magnetizing-sensing conditions.

One-cycle rms values of MAE demonstrate qualitatively similar dependence on the magnetizing frequency as compared with the hysteresis loss (see Figs. 1(b) and 6(a)). Therefore, there are similar nearly linear correlations between the MAE rms values and the hysteresis losses at $f_{mag} > 10$ Hz (see Figs. 5(a) and 6(b)). However, a low signal-to-noise ratio leads to a higher scattering of the MAE data. Correlation coefficients of the loss-separation fits are of the same level, $R = 0.991 - 0.996$; but the linear coefficients of the fits are higher $b/a \simeq \pm 1\%$. It is difficult to perform a detailed spectral analysis of the weak MAE signal; the reasonable signal-to-noise ratio is achieved by amplification within the resonance bandwidth of the MAE transducer. Number of the individual MAE pulses also drops hyperbolically

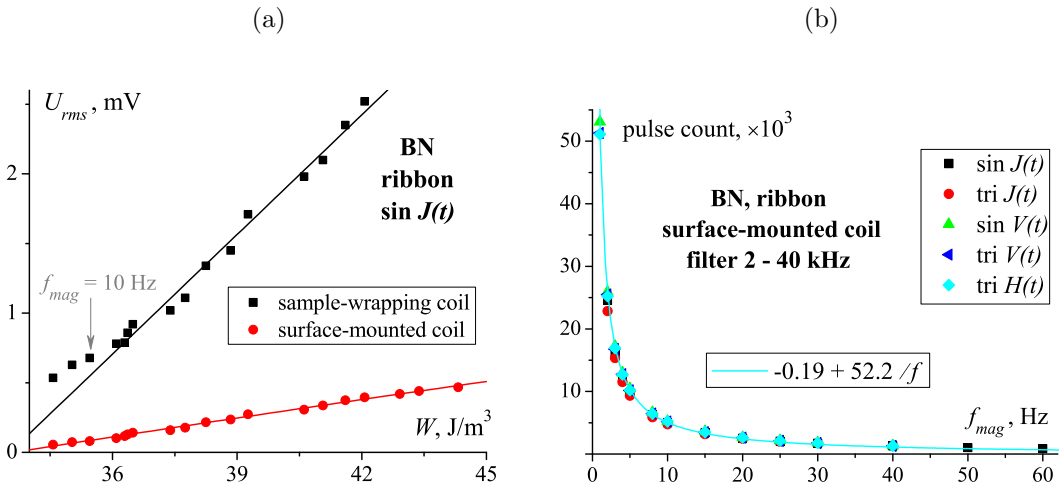

Figure 5: (a) Correlations between the BN rms values and the hysteresis losses under the sinusoidal $J(t)$ fitted by the linear curves for $f_{mag} > 10$ Hz. The BN signal from the Hitperm ribbon is filtered within the 10–40 kHz bandwidth. (b) Number of the BN individual pulses over a magnetization cycle versus f_{mag} fitted by the hyperbolical function with $R = 0.9998$.

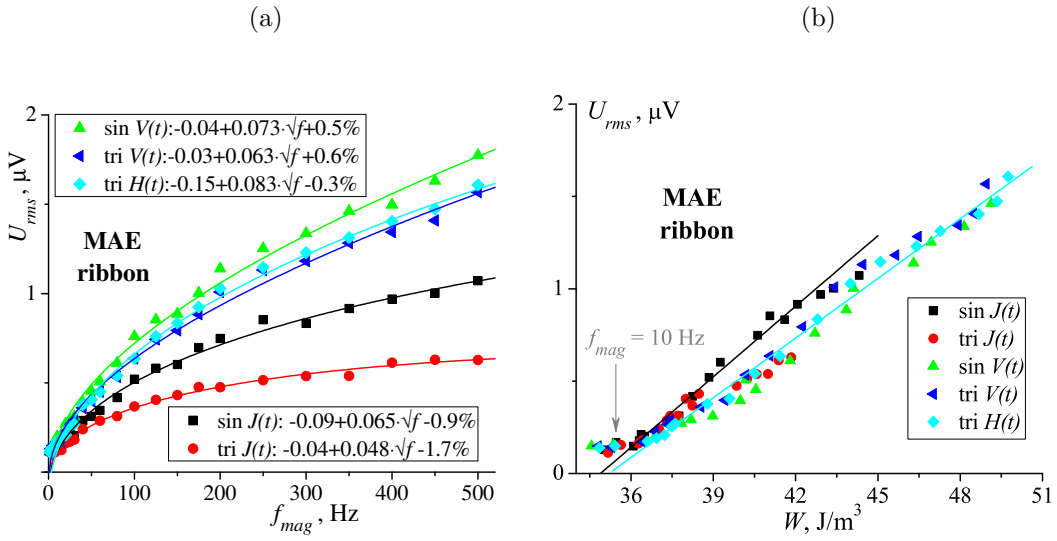

Figure 6: Dependence of the MAE rms value U_{rms} from the Hitperm ribbon on (a) the magnetizing frequency f_{mag} and (b) the hysteresis losses W for the different magnetizing waveforms. In (a) the relations are fitted by the loss-separation function with the linear coefficients showed in the labels as the percentage ratio b/a. In (b) the relations for the sinusoidal $J(t)$ and the triangular $H(t)$ are fitted by the linear curves for $f_{mag} > 10$ Hz.

with magnetizing frequency [4].

3.2. Electrical steels

Hysteresis loops for the tested electrical steels measured under the sinusoidal waveform of the magnetic induction $B(t)$ at the magnetizing frequency $f_{mag} = 50$ Hz are shown in Fig. 7(a) together with the quasi-static loop for the hardest NO steel. The loops are of typical sizes and shapes for this class of ferromagnetic materials [2]. The first GO steel with the dc coercive field $H_c \simeq 8$ A/m belongs to the softest transformer steels. Figure 7(b) presents dependence of the hysteresis loss on the magnetizing frequency obtained at the sinusoidal $B(t)$. The dependence are well fitted by the above-discussed

(a) (b)

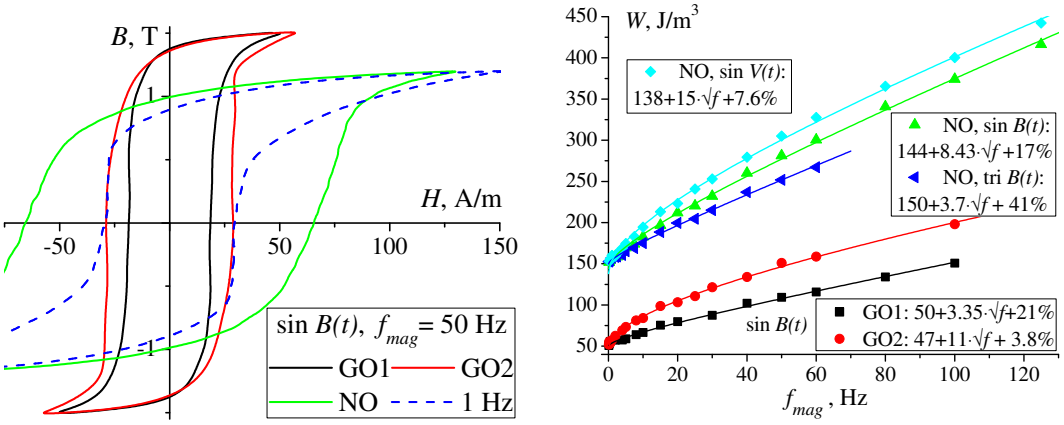

Figure 7: (a) Hysteresis loops $B(H)$ for the tested electrical steels at the sinusoidal induction waveforms $B(t)$ and the magnetizing frequency $f_{mag} = 50$ Hz. Nearly quasi-static loop obtained at $f_{mag} = 1$ Hz for the NO steel is shown for comparison. (b) Dependence of the hysteresis loss W on the magnetizing frequency f_{mag} for the tested steels at the sinusoidal $B(t)$. For the NO steel, similar dependence for the triangular $B(t)$ and the sinusoidal $V(t)$ are additionally shown. Relations are fitted by the loss-separation function. Linear coefficients of the fits are shown in the labels as the percentage ratio to the square root coefficients b/a.

(a) (b)

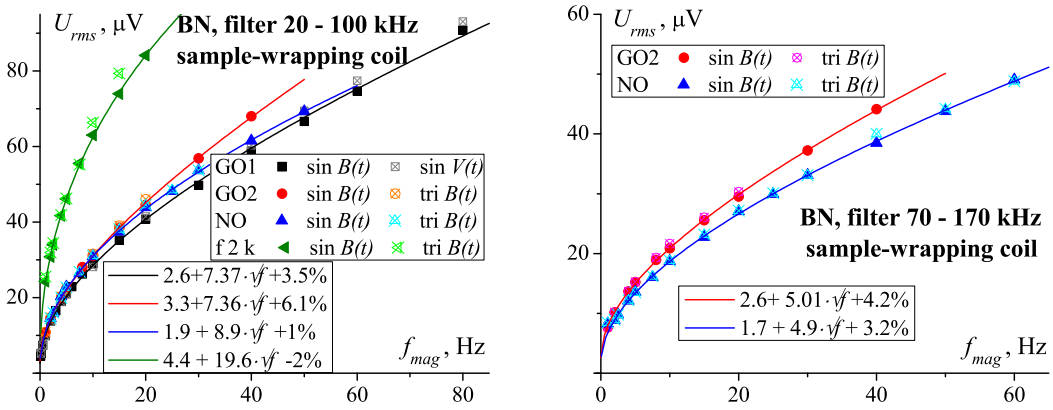

Figure 8: Dependence of the rms value U_{rms} of BN on the magnetizing frequency f_{mag} for the tested electrical steels and the different magnetizing waveforms. The BN signal is detected by the sample-wrapping coil and filtered within (a) the medium bandwidth 20–100 kHz and (b) the high bandwidth 70–170 kHz. In (a) the dependence obtained at the low filtering bandwidth 2–70 kHz is additionally shown for the NO steel (the highest green line). Relations are fitted by the same loss-separation function with the linear coefficients showed in the labels as the percentage ratio b/a; correlation coefficients of the fits are $R \simeq 0.9998$.

loss-separation formula $W = W_{dc} + a \cdot \sqrt{f_{mag}} + b \cdot f_{mag}$ as shown in the graph labels. Pearson correlation coefficients of the fits are $R \simeq 0.998$. Ratio between the fitting coefficients b/a is on a level of 20 % for the first GO and the NO steels, but is only 4 % for the second GO steel. Variations of the magnetizing waveform can significantly influence the slope of the loss-frequency dependence as shown in Fig. 7(b) for the NO steel. However, the slope differences are smaller for the GO steels. For the softest GO steel, there are the same loss-frequency relations for the triangular and the sinusoidal $B(t)$.

Figure 8 presents the dynamic rms dependence of BN detected by the sample-wrapping coil under different magnetizing waveforms and filtering bandwidths. The linear coefficients of the loss-separation fits for the two highest filtering bandwidths are on a level of $b/a \simeq 4\%$, which is several times higher than those for the tested ribbon (compare with Fig. 2). There is no evident correlation between magnitudes of the linear coefficient b for the hysteresis loss and the BN rms values. Moreover, the coefficient b is negative for the NO steel and the lowest filtering bandwidth. Influence of the magnetizing waveform shape on the BN rms value is practically negligible.

Figure 9 presents similar dynamic dependence of the BN rms value recorded by the surface-mounting coil. The low filtering bandwidths give small negative values of the linear coefficients of the loss-separation fitting, $b/a \simeq -1\%$, which is several times lower than those for the tested ribbon (compare Figs. 3(a) and 9(a)). However, the fittings for the GO steels and the high filtering bandwidth 70–170 kHz give $b/a \simeq +4\%$ (see Fig. 9(b)). There is again no evident correlation between the linear coefficients of the BN rms and the loss dependence as well as there is no noticeable influence of the magnetizing waveform shape on the BN rms values.

The Fourier power spectra of the BN signal behave correspondingly to the above-shown dynamic dependence of the rms value. There is a similar suppression of the $\sqrt{f_{mag}}$-normalized spectra in the low-frequency region leading to the negative linear coefficient of the loss-separation fits at the low filtering bandwidths (see Figs. 4(a), 9(a) and 10(a)). However, the last power spectrum for $f_{mag} = 50$ Hz in Fig. 10(a) does not already demonstrate such a suppression in the low-frequency region, but on the contrary, it

(a) (b)

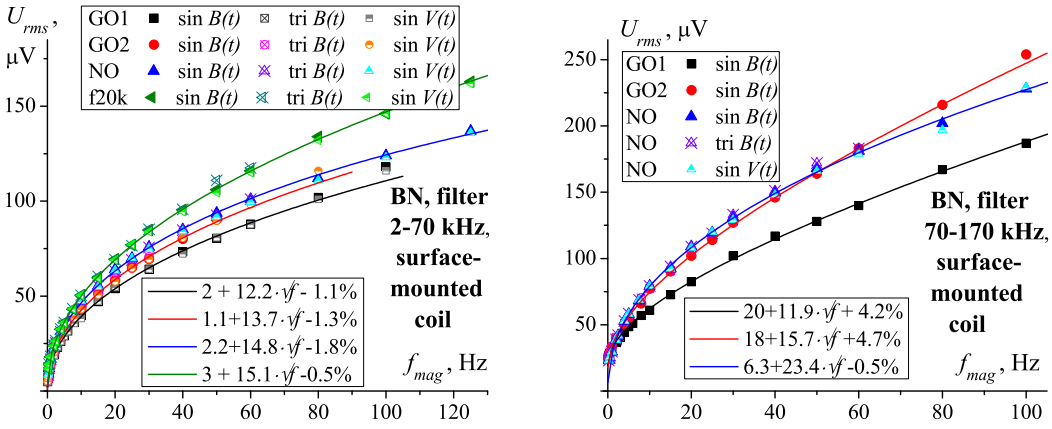

Figure 9: Dependence of the rms value U_{rms} of BN on the magnetizing frequency f_{mag} for the tested electrical steels and the different magnetizing waveforms. The BN signal is detected by the surface-mounted coil and filtered within (a) the low filtering bandwidth 2–70 kHz and (b) the high filtering bandwidth 70–170 kHz. In (a) the dependence obtained at the medium filtering bandwidth 20–100 kHz is additionally shown for the NO steel (the highest green line). Relations are fitted by the loss-separation function with the linear coefficients showed in the labels as the percentage ratio b/a; correlation coefficients of the fits are $R \simeq 0.9996$.

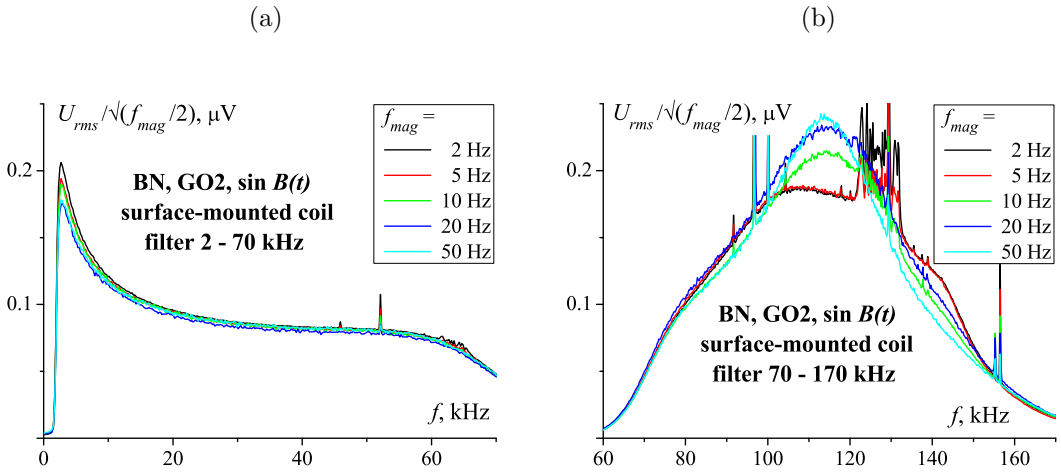

Figure 10: Fourier power spectra of the BN signals recorded by the surface-mounted coil at different filtering bandwidths: (a) 2–70 kHz; (b) 70–170 kHz. The measurements are performed for the second GO steel at the sinusoidal $B(t)$ waveform. Similar to Fig. 4(a), the spectra for $f_{mag} = 5 - 50$ Hz are normalized to $U_{rms}/\sqrt{f_{mag}/2}$.

shows a small rise as compared with the 20 Hz spectrum at higher frequencies $f \simeq 20 - 60$ kHz. This rise becomes apparent at frequencies ~ 100 kHz leading to the positive coefficient of the loss-separation fits at the high filtering bandwidth (see Figs. 9(b) and 10(b)). Peaks of the spectra near 120 kHz is determined by the resonance of the surface-mounted coil [9]. For such high frequencies, the signal-to-noise ratio is worse; the spectra are noisier with clear spikes of disturbing harmonics [13]. Dynamic dependence of the BN pulse count for the electrical steels are similar to that for the ribbon (see Fig. 5(b)).

For the softest GO steel, good linear correlations between the BN rms values and the hysteresis loss are observed for different measurement conditions in an ac magnetization range $f_{mag} > 5$ Hz (see Fig. 11(a)). For the

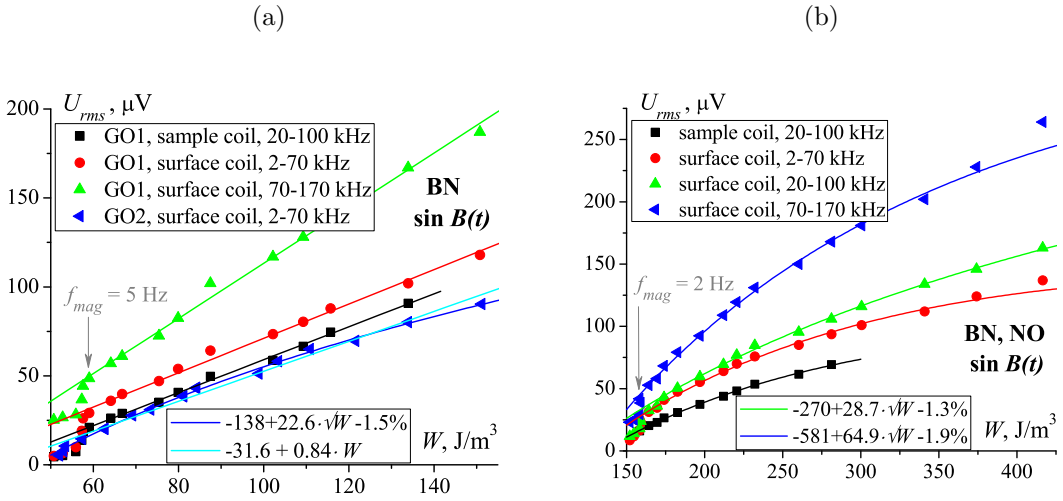

Figure 11: Correlations between the BN rms values and the hysteresis loss for the tested electrical steels. The measurements are made by both coils at the sinusoidal $B(t)$ and different filtering bandwidths. The data for the GO steels are fitted by the linear curves for $f_{mag} > 5$ Hz. The data for the second GO and the NO steels are fitted by the loss-separation function for $f_{mag} > 2$ Hz; correlation coefficients of the fits are $R \simeq 0.998$.

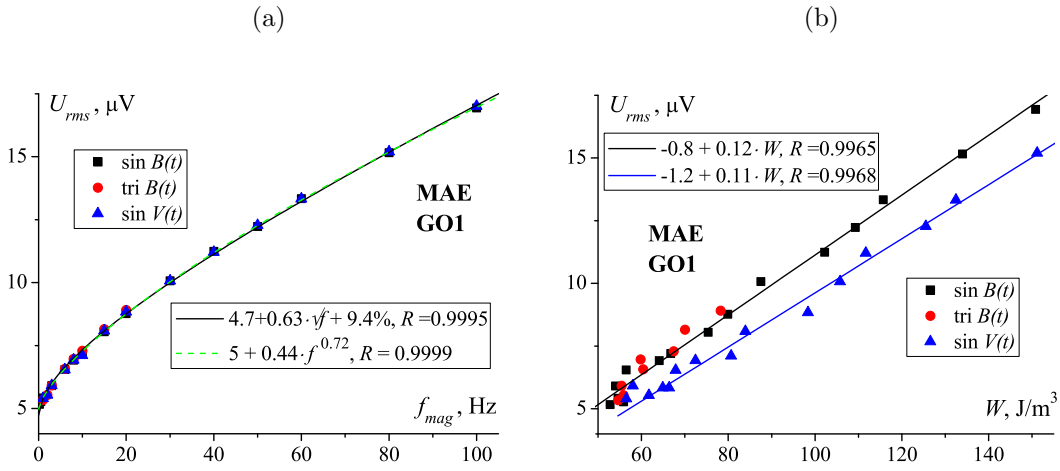

Figure 12: (a) Dependence of the rms value U_{rms} of MAE on the magnetizing frequency f_{mag} for the softest GO steel and the different magnetizing waveforms. The dependence is fitted by the loss-separation and the power functions with the comparable correlation coefficients R. (b) Linear correlations between the MAE rms values and the hysteresis loss for the same GO steel.

second GO steel, this correlation bends down to the loss scale and is better fitted by the same loss-separation function with a small linear coefficient $b/a = -1.5\%$; the correlation coefficient of this fit is $R = 0.9977$ versus the linear fit $R = 0.993$. For the NO steel, the correlations should be also fitted by the loss-separation function with the similar ratio b/a (see Fig. 11(b)). The observed $\sqrt{W}$-like relations are consistent with our previous results for other electrical steels with similar magnetic properties [14].

Figure 12 presents dependence of the MAE rms value on the magnetizing frequency and the hysteresis loss for the softest GO steel. There is again no evident influence of the magnetizing waveform shape on the rms value. The linear coefficient of the loss-separation fit $U_{rms}(f_{mag})$ is relatively high, $b/a = 9.4\%$, but it is still twice lower than that for the corresponding depen-

dence of the hysteresis loss (compare Figs. 7(b) and 12(a)). The constant term $U_{dc} \simeq 5$ μV is much higher than that for the ribbon measurements because of the wider filtering bandwidth (compare with Fig. 6(a)). The correlations between the MAE rms values and the hysteresis loss demonstrate the same linear trend, but in the whole f_{mag} range in contrast to the BN data (compare Figs. 11(a) and 12(b)). For the second GO steel, very similar results are obtained: $U_{rms} = 4.5$ μV$+0.98\cdot\sqrt{f_{mag}}+11\%$ and $U_{rms} = -1.44+0.121\cdot W$ for the sinusoidal $B(t)$ (see Fig. 4 in our recent work [4]). First, there are comparable ratios $b/a \simeq 10\%$ for the MAE dependence $U_{rms}(f_{mag})$ for both GO steels despite of quite different ratios $b/a = 21$ and 3.8% for the corresponding loss data. Second, a good linear correlation of the MAE rms values with the hysteresis loss for the second GO steel contradicts the corresponding BN data (see Fig. 11(a)).

4. Discussion

Hysteresis losses of magnetic ribbons are known to increase nearly proportional to $\sqrt{f_{mag}}$, although there is still no a clear explanation whether it is a consequence of their tiny thickness, high resistivity or specific DW structure [1, 5]. The studied nanocrystalline ribbon follows the same trend and the thickness is expected to be an important factor determining such a loss behavior (see Fig. 1(b)). Anyway, this factor is definitely important for investigation of the BN response: the tiny thickness ensures homogeneous magnetization and detection. But even under these measurement conditions, intensity of the BN signal behaves differently from the hysteresis loss. For the case of the sample-wrapping coil, a considerable positive level of the linear

coefficient b can be explained by influence of the high-frequency harmonics of the hysteresis induction signal since the high-frequency filtering decreases the linear term of the loss-separation fits to a negligible level (see Fig. 2). However, a negligible negative level of b for the case of the sample-mounted coil is evidently caused by a suppression of large BN pulses in the low-frequency part of the power spectra (see Figs. 3 and 4). These largest pulses are only sensitive to variations of the magnetizing waveform and are logically assigned to the magnetization reversal at the coercive field region, where considerable jumps of the 180° DW occur (see Fig. 1(a)). With increasing magnetizing frequency, number of the BN pulses is significantly reduced due to a pulse overlapping (see Fig. 5(b)). Such an overlapping is assumed to occur with a small loss in the total BN intensity, just as a peak of the differential magnetic permeability loses in its height with f_{mag} increase [6, 15].

For the electrical steels, the BN dynamic behavior is qualitatively similar to the above-discussed ribbon case despite the quite different dependence of the hysteresis loss [10]. There is no any correlation between the parameters of the loss-separation fits for the hysteresis losses and the BN rms values. There is much weaker influence of the magnetizing waveform shape on the BN rms value as compared with the hysteresis loss. Moreover, the dynamic rms dependence for three tested steels are very close to each other, which indicates a comparable level of the BN activity. For the low filtering bandwidth, the BN spectra demonstrate similar suppression of the low-frequency BN signal at $f \leq 20$ kHz giving the negative linear term of the loss-separation fits (see Figs. 8(a), 9(a) and 10(a)). Qualitatively similar results with higher $b/a \simeq -7\%$ are obtained in our previous work [6] for a harder microalloyed

steel with dc $H_c = 210$ A/m. There is only one significant distinction from the ribbon data. This is the high-frequency BN activity at $f \sim 100$ kHz leading to the positive b coefficient at the high filtering bandwidth, which can not be already explained by the high-frequency harmonics of the hysteresis signal (see Figs. 8(b) and 9(b)). This high-f BN activity is determined by short BN pulses and can be logically assigned to the hysteresis loop knees, where the 90° DW reorganization mostly occurs. These are prior and completion phases of the magnetization reversal, where nucleation, growth and subsequent annihilation of the 90° domains on the grain boundaries and the sheet surface take place. These domains are needed to close the internal magnetic flux of the rapidly moving 180° domains, thereby minimizing the magneto-static energy [16]. With increase of the magnetizing frequency, these knee-regions of the hysteresis loops do not significantly change, only the magnetization reversal occurs at higher magnetic fields producing wider $B(H)$ loops (see Figs. 1(a) and 7(a)). However, a number of the magnetic domains is known to rise at high $f_{mag} \geq 40$ Hz for this class of materials [17]. Increasing number of the 90° DWs can cause this additional BN activity at $f \sim 100$ kHz giving the positive linear coefficient b for the high filtering bandwidth.

The principal issues under discussion are validity and physical grounds of the observed dynamic dependence with the $\sqrt{f_{mag}}$ dominant term. We use the loss-separation formula to fit the micro-magnetic signals simply by analogy with the hysteresis data. There is still no suitable theory for describing the obtained dynamical properties of BN/MAE, which we can rely on [18, 19, 20]. We also try to use the power function proposed in [11, 12] as a fitting alternative. It provides a similar accurate fitting of the experimental

data, but the power coefficient can significantly deviate from the expected value 0.5, even if the corresponding loss-separation fitting gives a small ratio b/a (see Fig. 3(b) and 12(a)). Analysing the BN spectra in Figs. 4 and 10, we are inclined to stick with the opinion about the dominating role of the $a \cdot \sqrt{f_{mag}}$ component with the above-discussed deviations, which can be introduced by the linear term $\pm b \cdot f_{mag}$. Physical background should be of similar origin as proposed to explain the excess loss W_{ex} component. Rapid irreversible changes of local magnet moments caused by the DW motion are detected by the induction coils with an unknown transfer coefficient [19]. After the filtering (it should be mentioned that a coil with many turns of winding has a self-capacitance and is a LC filtering circuit in fact), the detected packet of the electrical impulses is symmetrical in polarity, so evaluation of the rms value is a routine method to estimate the intensity of the micro-magnetic signals [9]. These sensing-evaluation procedures could also have an influence on the resulting dynamic dependence, but we again stick with the opinion about the micro-magnetic origin of the observed $U_{rms} \sim \sqrt{f_{mag}}$ behavior. The local DW motion does not only give rise to the BN activity, but also to micro eddy-currents, which are considered to define the excess loss $W_{ex} \sim \sqrt{f_{mag}}$ term [1, 2].

Small negative ratios $b/a \simeq -1\%$ for the MAE $J(t)$-controlled dependence of the ribbon in Fig. 6(a) can be similarly explained by the overlapping of the largest MAE pulses because the magnetization rates near H_c are minimal under the $J(t)$ adjusted waveforms [6]. Much higher positive ratios $b/a \simeq 10\%$ for the MAE dependence of the GO steels as compared with the corresponding BN relations (see Figs. 8, 9(b) and 12(a)) can be explained

by a more intensive MAE response to the 90° DW activity. As mentioned in Introduction, theoretically MAE should not be sensitive to the motion of the 180° DWs at all [3, 4]. The next factor, which can be responsible for higher MAE ratios b/a, is the fact that the MAE waves freely propagate through the whole material, whereas the surface-mounted coil picks up the BN signal from the steel surface only [4, 9]. However, the thickness of the GO steel sheets is still small enough to ensure relatively homogeneous magnetization and BN detection.

Finally, let us discuss the observed correlations between the micro-magnetic rms values and the hysteresis losses. A main difference between these parameters is caused by the reversible component of the magnetization reversal describing by the loss-separation terms W_{dc} and $W_{cl} \sim f_{mag}$. The constant terms W_{dc}/U_{dc} and different near-dc magnetization dynamics on the macro- and the micro-scales are probably responsible for a lack of the correlation at low $f_{mag} \leq 2 - 10$ Hz. At higher dynamic range, the correlations actually proves the physical coupling of the micro-magnetic signals (local DW motions causing the detected magnetic pulses) with the exchange losses $W_{ex} \sim \sqrt{f_{mag}}$ assigned to the micro eddy currents [1]. This assumption is experimentally confirmed by the linear correlations in case of all MAE data and the BN data for the two softest and thinnest materials, the ribbon and the first GO steel (see Figs. 5(a), 6(b), 11(a) and 12(b)). The square-root correlations for the two harder and thicker materials, the second GO and the NO steels, are defined by a near-linear dependence $W \sim f_{mag}$ at high $f_{mag} > 20$ Hz (see Figs. 7(b) and 11).

5. Conclusion

The dynamic behavior of magnetic Barkhausen noise and magneto-acoustic emission for the typical soft ferromagnetic materials is primarily determined by a square root of the magnetizing frequency. However, a supplementary linear term could be added to fit the experimental dependence of the rms intensities of these micro-magnetic signals (by analogy with the hysteresis loss separation). For the Barkhausen noise data, this linear term is mostly negligible. Its sign, however, is opposite for different regions of the Fourier spectrum. It is negative for the largest impulses at the frequencies up to $f \leq 20$ kHz, but seems to be positive for the short impulses at $f \sim 100$ kHz. For the magneto-acoustic emission, the linear terms of the fits become considerable and comparable with the classical hysteresis loss components. This gives a good linear correlation between the hysteresis loss and the rms intensity of the magneto-acoustic emission. No direct correlation is found between the fitting parameters for the micro-magnetic and the macro-hysteresis responses, however, related physical factors (local domain wall motion and attendant micro eddy currents) are assumed to be responsible for the square root rise of the dynamic dependence. Influence of the magnetizing waveform shape on the micro-magnetic rms intensities is nearly negligible as compared with that on the hysteresis loss.

Acknowledgment

The authors appreciate the financial support of the Czech Science Foundation (GA ČR) under projects 13-18993S and 14-36566G. The authors thank

Dr. P. Švec from Institute of Physics SAS in Bratislava and Dr. P. Anderson from Cardiff University for sample provision.

References

[1] A.J. Moses, Energy efficient electrical steels: Magnetic performance prediction and optimization, Scripta Mater. 67 (2012) 560–565.

[2] S.E. Zirka, Y.I. Moroz, R.G. Harrison, K. Chwastek, On physical aspects of the Jiles-Atherton hysteresis models, J. Appl. Phys. 112 (2012) 043916.

[3] M. Guyot, V. Cagan, The magneto-acoustic emission (invited), J. Appl. Phys. 73 (1993) 5348–5353.

[4] A. Stupakov, O. Perevertov, M. Landa, Dynamic behaviour of magneto-acoustic emission in a grain-oriented steel, J. Magn. Magn. Mater. 426 (2017) 685-690.

[5] C.D. Graham Jr, Physical origin of losses in conducting ferromagnetic materials (invited), J. Appl. Phys. 53 (1982) 8276–8280.

[6] A. Stupakov, O. Perevertov, V. Zablotskii, Dynamical properties of magnetic Barkhausen noise in a soft microalloyed steel, IEEE Trans. Magn. 51 (2015) 6100204.

[7] O. Stupakov, P. Švec, Three-parameter feedback control of amorphous ribbon magnetization, J. Electr. Eng. 64 (2013) 166–172.

[8] A. Stupakov, O. Perevertov, V. Zablotskii, A system for controllable magnetic measurements of hysteresis and Barkhausen noise, IEEE Trans. Instrum. Measur. 65 (2016) 1087–1097.

[9] O. Stupakov, J. Pal'a, T. Takagi, T. Uchimoto, Governing conditions of repeatable Barkhausen noise response, J. Magn. Magn. Mater. 321 (2009) 2956-2962.

[10] O. Stupakov, Y. Melikhov, Influence of magnetizing and filtering frequencies on Barkhausen noise response, IEEE Trans. Magn. 50 (2014) 6100104.

[11] A. Zhukov, M. Vázquez, J. Velázquez, C. García, R. Valenzuela, B. Ponomarev, Frequency dependence of coercivity in rapidly quenched amorphous materials, Mater. Sci. Eng. A A226–228 (1997) 753–756.

[12] R. Grössinger, N. Mehboob, D. Suess, R. Sato Turtelli, M. Kriegisch, An eddy-current model describing the frequency dependence of the coercivity of polycrystalline galfenol, IEEE Trans. Magn. 48 (2012) 3076–3079.

[13] M. Vashista, V. Moorthy, Influence of applied magnetic field strength and frequency response of pick-up coil on the magnetic Barkhausen noise profile, J. Magn. Magn. Mater. 345 (2013) 208-214.

[14] O. Stupakov, Local non-contact evaluation of the ac magnetic hysteresis parameters of electrical steels by the Barkhausen noise technique, J. Nondestruct. Eval. 32 (2013) 405–412.

[15] O.V. Perevertov, Application of the Preisach model to the magnetization process in steels, J. Phys. D: Appl. Phys. 35 (2002) 2467–2471.

[16] O. Perevertov, J. Thielsch, R. Schäfer, Effect of applied tensile stress on the hysteresis curve and magnetic domain structure of grain-oriented transverse Fe-3%Si steel, J. Magn. Magn. Mater. 385 (2015) 358-367.

[17] T.R. Haller, J.J. Kramer, Observation of dynamic domain size variation in a silicon-iron alloy, J. Appl. Phys. 41 (1970) 1034–1035.

[18] G. Biorci, D. Pescetti, Frequency spectrum of the Barkhausen noise, J. Appl. Phys. 28 (1957) 777–780.

[19] G. Bertotti, F. Fiorillo, M.P. Sassi, Barkhausen noise and domain structure dynamics in Si-Fe at different points of the magnetization curve, J. Magn. Magn. Mater. 23 (1981) 136-148.

[20] R.G. Harrison, Accurate mean-field modeling of the Barkhausen noise power in ferromagnetic materials, using a positive-feedback theory of ferromagnetism, J. Appl. Phys. 118 (2015) 023904.